View metadata, citation and similar papers at core.ac.uk
brought to you by CORE
provided by White Rose Research Online

Mapping Nanostructural Variations in Silk by Secondary Electron Hyperspectral Imaging

*Quan Wan, Kerry J. Abrams, Robert C. Masters, Abdullah C. S. Talari, Ihtesham U. Rehman, Frederik Claeyssens, Chris Holland, and Cornelia Rodenburg**

Nanostructures underpin the excellent properties of silk. Although the bulk nanocomposition of silks is well studied, direct evidence of the spatial variation of nanocrystalline (ordered) and amorphous (disordered) structures remains elusive. Here, secondary electron hyperspectral imaging can be exploited for direct imaging of hierarchical structures in carbon-based materials, which cannot be revealed by any other standard characterization methods. Through applying this technique to silks from domesticated (*Bombyx mori*) and wild (*Antheraea mylitta*) silkworms, a variety of previously unseen features are reported, highlighting the local interplay between ordered and disordered structures. This technique is able to differentiate composition on the nanoscale and enables in-depth studies into the relationship between morphology and performance of these complex biopolymer systems.

A polymer's macroscopic material properties depend on the local organization of its nanostructures.[1,2] For silk, a key factor in this relationship appears to be the ability to modulate crystallinity, also referred to as the ordered fraction.[3] While this ordered fraction has been measured in bulk through spectroscopy (Raman,[4a–f] nuclear magnetic resonance (NMR),[4g,h] circular dichroism (CD),[4i,j] small angle X-ray scattering (SAXS),[4k,l] small angle neutron scattering (SANS),[4m,n] and Fourier transform infrared (FTIR)[4o–r]) and inferred via mechanical testing (tensile, dynamic mechanical thermal analysis (DMTA)),[4s–v] modeling suggests that the mechanical properties of silks are a rather complex interplay between ordered and disordered fractions at a local scale.[5]

While some studies have indicated spatial differences of these fractions, either through radiolabeling[6] or local modulus measurements,[7] few, if any, techniques have been able to map this nanocompositional variation directly. This situation represents a current length-scale characterization and knowledge gap.

This work exploits secondary electron hyperspectral imaging (SEHI), a new scanning electron microscope (SEM)-based characterization tool to reveal and visualize nanostructural variations across micron-scale spatial dimensions. We report that despite similarity in overall ordered fraction, there are distinct differences in the nanoscale order/disorder maps of natural silk fibers from both *Bombyx mori* and *Antheraea mylitta*.

The structural hierarchy of silkworm silks surrounds a sericin glue that binds two microscopic fibroin brins (≈15 µm),[3] which are comprised of ≈200 nm microfibers and nanofibrils[8] and, finally, nanoscale phases, which can be ordered or disordered,[4] as shown in the schematic diagram in **Figure 1**a.

Using low-voltage standard SEM of a cryo-snapped and plasma-exposed silk fibers of *B. mori* silk and *A. mylitta* silk, it is possible to visualize bright nanostructures (Figure 1a) due to topographical contrast, but such contrast is problematic for accurate nanoscale dimension measurements due to a feature size- and shape-dependent edge effect.[9] Furthermore, the topography can be caused by different mechanisms, and it is therefore prone to artefacts introduced by sample preparation. Nevertheless, we observe that the average area fraction of these nanostructures is similar in both silks, however in *A. mylitta* silk, the round nanostructures seem smaller, denser, and interconnected.

In order to determine the nature of these bright nanostructures and their dimensions, we applied SEHI. SEHI exploits the distinctiveness of secondary electron (SE) signals in carbon-based material[10] for hyperspectral imaging (HI) and has the advantage of being able to avoid the confounding influence of topology, which beleaguers standard SEM (see Section S6 in the Supporting Information). The concept of HI is well established in vibrational spectroscopies,[11a] where images are formed from several different energy regions, and based on distinctive peaks in the spectrum. This is demonstrated in the schematic in Figure 1d. Here we collect SE spectra from the high-density nanoscale regions, as established by comparison of backscattered electron density maps[12] (Section S1, Supporting Information), which we find correlate with the bright features in the standard SEM images in Figure 1a. This allows us to investigate which peaks in the SE spectra are related to high density (Section S3, Supporting Information), and thus to high order (Section S1, Supporting Information). We then apply the HI concept to quantitatively map the different phases in silks by imaging with an energy window of 3.9 ± 0.3 eV which was specifically selected to map high-order regions and is free from topographical artefacts

Q. Wan, Dr. K. J. Abrams, R. C. Masters, Dr. A. C. S. Talari, Dr. I. U. Rehman, Dr. F. Claeyssens, Dr. C. Holland, Dr. C. Rodenburg
Department of Materials Science and Engineering
University of Sheffield
Sir Robert Hadfield Building, Mappin Street, Sheffield S1 3JD, UK
E-mail: c.rodenburg@sheffield.ac.uk

© 2017 The Authors. Published by WILEY-VCH Verlag GmbH & Co. KGaA, Weinheim. This is an open access article under the terms of the Creative Commons Attribution License, which permits use, distribution and reproduction in any medium, provided the original work is properly cited.

DOI: 10.1002/adma.201703510

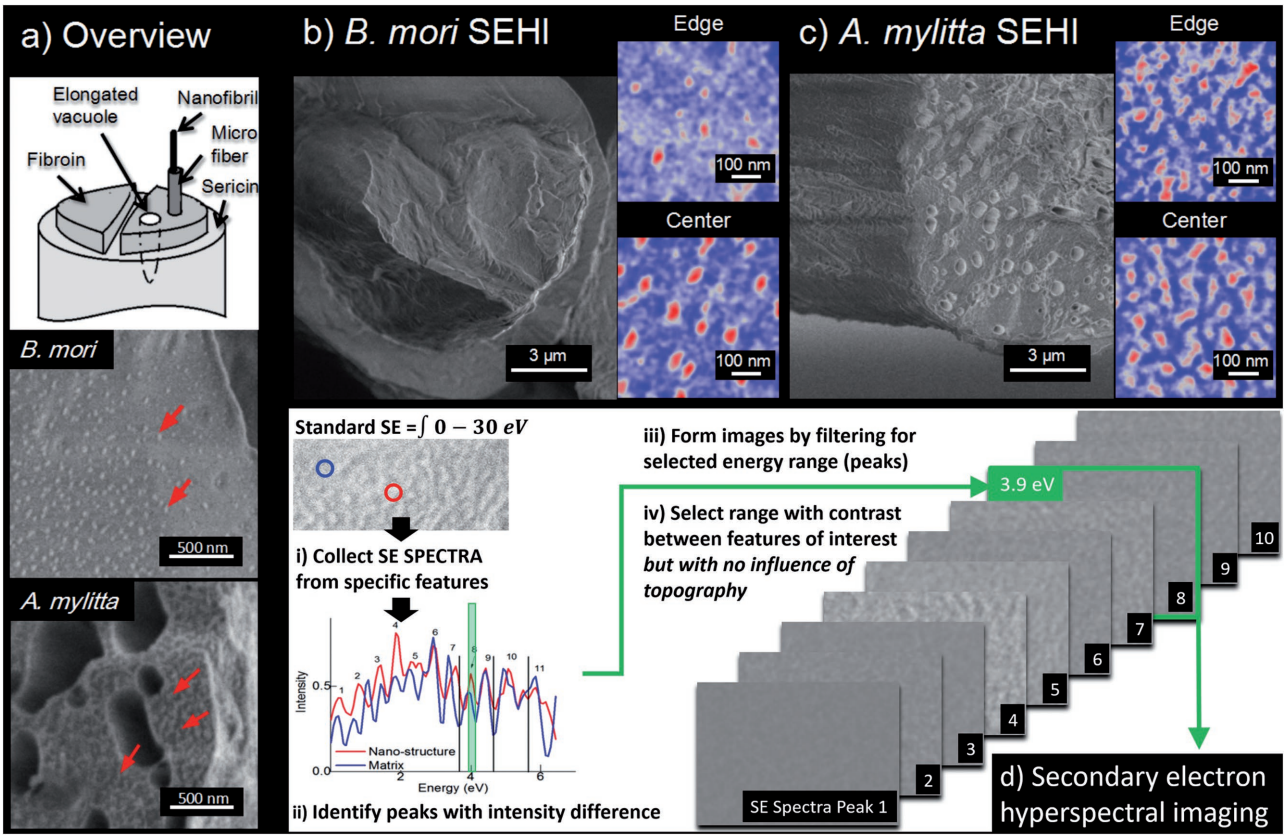

Figure 1. a) A schematic overview of a silkworm silk fiber and cross-sectional micrographs of *B. mori* and *A. mylitta* silk using low-voltage SEM which identifies bright nanostructures on cryo-snapped, plasma-etched cross-sections as shown by red arrows. Here the nanostructures are visible due to topography contrast as they are slightly raised due to the preferential removal of the low-order matrix during sample preparation. Using SEHI, topographical contrast can be supressed (Sections S3 and S6, Supporting Information) and the bright features in a) are identified as the ordered fraction (Sections S3 and S5, Supporting Information) and shown in fiber cross-sections for b) *B. mori* and c) *A. mylitta*. For better visualization of these structures, an enlarged view (500 nm × 500 nm) at the ordered fraction energy peak along with color coded SE hyperspectral image collected using the energy window 3.9 ± 0.3 eV is shown taken from the edge and from the center for each species. Red is assigned to the ordered phase, Blue is the disordered phase and gray the oriented amorphous phase. The concept of SEHI is summarized in the schematic in d), which displays the SE spectra from B. *mori* silk. The spectra for *A. mylitta* silk are shown in Figure S3 (Supporting Information) along with a full explanation of the terminology in Section S1 (Supporting Information).

(see the Supporting Information for energy calibration (Section S2), peak selection, and validation (Section S3)). To demonstrate the close relation of HI to vibrational spectroscopy, we performed SEHI on a semi-crystalline polymer system in conjunction with Raman microscopy to further confirm the validity and suitability of our technique for silks (Section S4, Supporting Information).

Raman/infrared (IR)[11a–c] and X-ray diffraction (XRD)[11d] studies show that at least two dominating phases[11e] exist in silk fibroin: a crystalline phase, mostly assembled of β-sheet crystals, that we term ordered and an amorphous phase that we classify as disordered. A third, oriented amorphous phase has also been suggested based on Raman and XRD studies on spider silks,[13a,b] and inferred for *B. mori* silk from the oriented chain composition in the matrix and in regenerated samples.[13c,d]

To confirm the most appropriate energy window that was used to discriminate the ordered phase, we first analyzed each of 11 observed peaks in the SE spectra (Figure S3, Supporting Information) in terms of peak position, and peak intensity differences between matrix and nanostructures to predict a suitable peak for imaging (Figure S4, Supporting Information), and then tested this prediction by obtaining SEHI images for each of the peaks present in the collected SE spectra (Figure S5, Supporting Information). From the analysis of spectra only, we predicted that the window at 3.9 ± 0.3 eV is most suitable to image high-order regions, which was confirmed by the obtained SEHI image array shown in Figure S5 (Supporting Information).

A phase map of the ordered fraction for these materials is presented in **Figure 2**. Here high intensity (white) corresponds to the ordered phase, mid-intensity (mid-gray levels) to the oriented amorphous phase, and low intensity (black) to the disordered phase based on fitting Gaussian peaks to the strongly asymmetric histograms (Figure 2e,f) that can be best fitted by three peaks (please see full details for peak fitting and justification of phase allocation in Section S5 in the Supporting Information). Note that this phase–contrast relationship is only valid for the 3.9 eV SEHI image. In fact, we find that for SEHI, using a window centered at 4.2 eV of the same area results in a reversal of contrast at most locations as shown in **Figure 3**. Hence, we attribute the 4.2 eV peak in the SE spectrum to the disordered phase (see Section S3 in the Supporting Information for full justification).

© 2017 The Authors. Published by WILEY-VCH Verlag GmbH & Co. KGaA, Weinheim

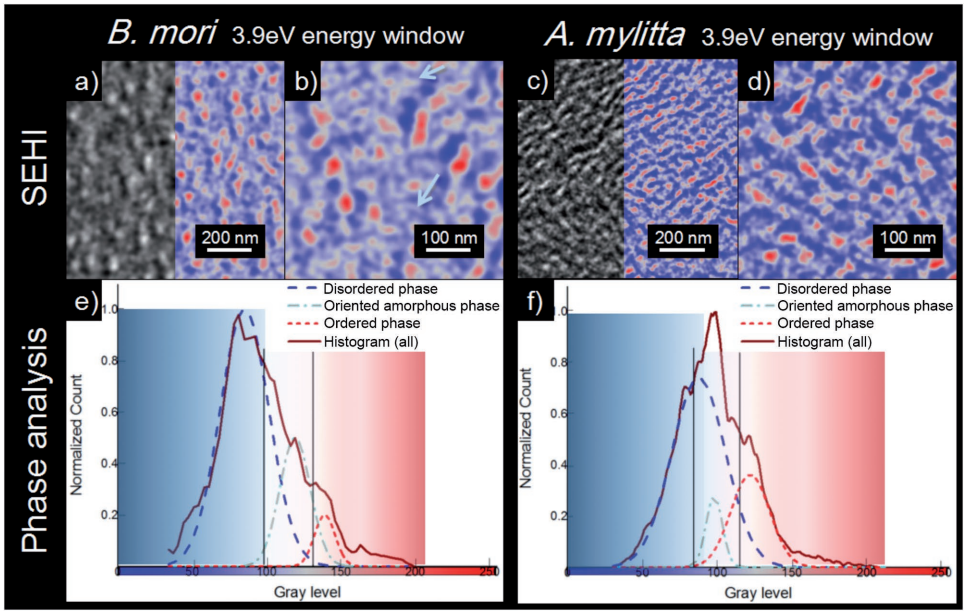

Figure 2. Half color coded SEHI image energy window 3.9 ± 0.3 eV for a) *B. mori* silk and c) *A. mylitta* silk cryo-snapped cross-section, with higher magnification and full color coding SEHI in b) and d). The 3.9 ± 0.3 eV energy window results in high-intensity levels for the ordered phase (Sections S3 and S5, Supporting Information). Therefore, in image a–d), red represents the ordered phase, blue is the disordered phase and the gray represents the oriented amorphous phase (examples marked by arrows). To assign these colors the histogram of the original gray scale SEHI image was analyzed in e) for *B. mori* silk and f) for *A. mylitta* silk with the peak of each phase calculated through Gaussian fitting to match the overall histogram (for full details of peak fitting see Section S5 in the Supporting Information).

To determine the bulk ordered fraction for *B. mori* silk and *A. mylitta* fibers, we further analyzed the 3.9 ± 0.3 eV SEHI images as a whole (details in Section S5 in the Supporting Information). By assuming that the silk proteins in the bright ordered phase adopt mostly β-sheet conformations and form nanoscale crystals, as suggested by literature,[14] based on total area fraction for *B. mori*, we estimate an overall fiber ordered content of ≈10.4%, which agrees well with ≈10% crystallinity as measured by X-ray data.[15] For *A. mylitta* fibers, an ordered content of ≈13.4% is estimated, which is close to reports of ≈14.7% β-sheet content as determined by IR spectroscopy.[11f]

Moving beyond bulk measurements, SEHI phase mapping reveals that the size and distribution of the ordered structures are not uniform across the silk fiber cross-section (Figure 1). The local ordered phase maps of *B. mori* (Figure 1b) shows that the diameter of these ordered structures is larger near the edge of the fiber in comparison to the size of the order structures found in the fiber center. The related full size distribution analysis across the whole cross-section is shown in Figure S11c (Supporting Information), and the SEHI data reveal an increase from ≈25 to 45 nm within the first 800 nm for *B. mori*. Likewise, the area fraction reaches a maximum of 12% at the center of the fiber see Figure S11h (Supporting Information). In contrast, *A. mylitta*'s ordered fraction maps (Figure 1c) did not show any significant size change across the fiber, maintaining a diameter of 40 nm as shown in Figure S11f (Supporting Information), and an overall decrease of ordered structures toward the center of the fiber (see Figure S11h in the Supporting Information). However, these distribution differences may be related to the presence of the large amount of small vacuoles close to the fiber edge for *A. mylitta* (Section S7, Supporting Information).

The observed change in ordered fraction across the fiber in *B. mori* is consistent with a model proposed by transmission electron microscope (TEM) analysis of degummed *B. mori* silk, whereupon crystalline areas are reported to form cup-shaped banded regions along the longitudinal axis.[15] This is also reflected in the inclined nanopattern observed on the longitudinal section of *B. mori* silk (see Figure S13 in the Supporting Information). Due to the absence of ordered structure size variation in our *A. mylitta* samples, we also infer the absence of cup-shaped banding, which is again confirmed by the relatively flat appearance of the areas between vacuoles in the longitudinal sections of *A. mylitta*. In summary, SEHI has revealed that despite having similar overall ordered phase fractions, these two species differ in both size and distribution of the ordered structures at the nanoscale.

Hence from our SEHI observations, we propose two main areas for hypothesis testing in the future. First, the distribution of order/disorder may be related to the flow field encountered by the silk feedstock in the gland as it undergoes solidification, and, second, this distribution may be related to a fiber's mechanical properties and failure mechanism.

Taking each area in turn, during spinning and in ex vivo rheological testing, the flow field encountered by the silk proteins is largely responsible for the formation and stabilization of ordered structures, specifically β-sheets and larger nanofibrils.[16] From the data presented here, *A. mylitta* adopts a more homogeneous size distribution of ordered features across the fiber, while *B. mori* ordered features are fewer and smaller at the fiber edge; we predict that the flow fields responsible for their generation are more evenly distributed in *A. mylitta* than in *B. mori*. This may be related to differences in gland

© 2017 The Authors. Published by WILEY-VCH Verlag GmbH & Co. KGaA, Weinheim

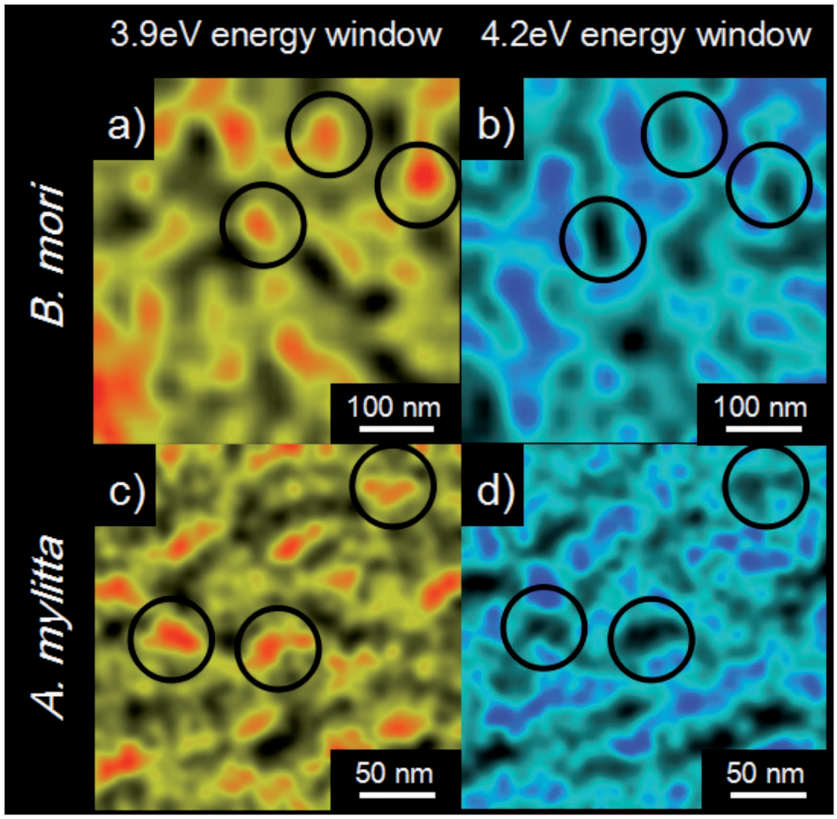

Figure 3. Color coded SEHI images collected from the 3.9 ± 0.3 eV ordered phase energy window a,c) are compared to the 4.2 ± 0.3 eV disordered phase energy window b,d) for *B. mori* and *A. mylitta* silk cross-section samples. Note the field of view for each species is the same for both images. The black circles represent areas where the intensity in the 3.9 ± 0.3 and 4.2 ± 0.3 eV windows are mutually exclusive, supporting our assignment of these windows to discriminate between ordered and disordered fractions.

morphology and the action of the silk press,[17a,b] the effects of sericin,[17c,d] or the feedstock's rheological properties facilitating a greater extensional flow in the middle of the silk duct of *B. mori*.[17e–j]

Finally, silk fiber mechanical properties are known to be species dependent and often correlated to their bulk crystallinity content.[18] Our results for ordered bulk content align well with those of previous spectroscopy studies;[11f,14] therefore, SEHI could support future structure–function work by probing how the ordered/disordered phases contribute toward a fiber's mechanical properties. For example, previous fractographic studies of typical polymer nanocomposites report that nanofibrous structures are generally tougher than the bulk component[19a–d] as has been proposed in modeling studies of silk.[19e,f] Hence this technique could be used to identify both the presence of and order/disorder content of silk nanofibrils.[8] However, at a slightly larger length scale, it is known that microvoids (i.e., the elongated vacuoles) may prevent stress concentrations and subsequent crack propagation in silk[20] and as such there may be a complex dynamics between impinging structural hierarchies, which remains to be elucidated.

In conclusion, SEHI has provided a means to spectroscopically map silk's molecular order and disorder across several length scales, down to the nano scale. We propose this new tool could provide us with a means to visualize a silks feedstock's flow history or be used as a predictor of a fiber's mechanical properties. Thus, we expect that this innovative approach will prove fundamental to the understanding of silk formation and indeed, other hierarchical materials.

Experimental Section

Silk cocoons were obtained from animals bred in captivity and supplied by World Wide Butterflies Ltd and stored under lab conditions until use. Cocoons were unraveled onto spools. *A. mylitta* samples were first demineralized by immersion for 48 h in 10 M ethylene diamine tetra acetic acid, gently stirred at 40 °C and unraveled at 20 mm s^{-1} in deionized water alongside *B. mori* cocoons (which do not require demineralization).

Subsequently, silk fibers were cut into 5 cm sections using a scalpel blade, and both ends were attached to a clean 1 cm x 3 cm silicon wafer by conductive carbon tape. The fixed fibers were soaked in deionized water and sandwiched between another silicon wafer before cryo-fracturing in liquid nitrogen. The "snapped" cross-section samples were left to dry in air at room temperature for over 2 h and then briefly plasma etched in a Diener Zepto version B plasma cleaner at 50% power of 100 W for 40 s. This treatment also enhances crystalline features and conductivity at the surface, which allows for better imaging.[21] The silk samples were not coated by a conductive coating before analysis, and artefacts created by plasma and electron beam damage is discussed and excluded in Section S8 in the Supporting Information.

According to the literature,[22] the SE spectra of many inorganic materials reflect the status/composition of material within the range of 0–12 eV SE energy. For silkworm silks, the spectra were collected with a similar method described in previously published work[23] utilizing deflection voltages 0–30 V in the through lens detector (TLD) in a Nova 450 nano-SEM, the detail of the filter mechanism in this detector was described in literature.[23] The SE hyperspectral images were collected by an iFast auto collection recipe for both SEMs, the image processing, and related SE spectra collection/peak selection is described in the previous paragraph and in Sections S2 and S3 in the Supporting Information, respectively. The 0–11 eV range was collected for the two silk species with an electron energy step size of 0.071 eV. The intensity data were averaged from several (2 × 2) μm^2 area on three different fibroin samples.

After identification of peaks in the SE spectra, the start and end of each peak was defined. The midpoint was defined as where the differentiated spectra reached zero. High-resolution SE images were taken at those equivalent deflection voltages and processed by subtracting the peak-end image from the peak-start image. The SEM image was contrast enhanced and normalized with software ImageJ v1.48, the original image for SEHI is shown in detail in Figure S8 (Supporting Information).

Supporting Information

Supporting Information is available from the Wiley Online Library or from the author.

© 2017 The Authors. Published by WILEY-VCH Verlag GmbH & Co. KGaA, Weinheim

Acknowledgements

The authors would like to thank C. Jiao, M. Uncovsky, and T. Vystavel of Thermo Fisher Scientific, Materials & Structural Analysis (formerly FEI) for the support with SEM software and J. Moffat and C. Holliday of Innovia Films for providing the polypropylene material applied in technique validation. Q.W. would like to thank the Sorby Centre for Microscopy and Microanalysis for the access to the electron microscope and related equipment; C.R. and K.A. would like to thank EPSRC for support under EP/N008065/1; C.H. would like to thank EPSRC for support under EP/K005693/1; and R.M. would like to thank the Grantham Centre for Sustainable Futures and the Faculty of Engineering at the University of Sheffield for providing a PhD studentship.

Conflict of Interest

The authors declare no conflict of interest.

Keywords

imaging, polymers, proteins, SEM, silks

Received: June 23, 2017
Revised: August 29, 2017
Published online:

[1] a) W. Zeng, L. Shu, Q. Li, S. Chen, F. Wang, X. M. Tao, *Adv. Mater.* **2014**, *26*, 5310; b) I. Zlotnikov, E. Zolotoyabko, P. Fratzl, *Prog. Mater. Sci.* **2017**, *87*, 292.

[2] a) M. J. Buehler, M. J. Cranford, *Nanotechnol., Sci. Appl.* **2010**, *3*, 127; b) P. Fratzi, in *Learning from Nature How to Design New Implantable Biomaterialsis: From Biomineralization Fundamentals to Biomimetic Materials and Processing Routes*. NATO Science Series II: Mathematics, Physics and Chemistry, Vol. *171* (Eds: R. L. Reis, S. Weiner), Springer, Dordrecht, The Netherlands **2014**, pp 15–34.

[3] a) Z. Shao, F. Vollrath, *Nature* **2002**, *418*, 741; b) G. Zhou, Z. Shao, D. P. Knight, J. Yan, X. Chen, *Adv. Mater.* **2008**, *21*, 366; c) N. V. Bhat, G. S. J. Nadiger, *Appl. Polym. Sci.* **1980**, *25*, 921; d) Y. Shen, M. A. Johnson, D. C. Martin, *Macromolecules* **1998**, *31*, 8857; e) R. Gebhardt, C. Vendrely, M. Burghammer, C. Riekel, *Langmuir* **2009**, *25*, 6307; f) C. Holland, D. Porter, F. Vollrath, *MRS Bull.* **2013**, *38*, 73; g) A. Koeppel, C. Holland, *ACS Biomater. Sci. Eng.* **2017**, *3*, 226.

[4] a) P. Monti, P. Taddei, G. Freddi, T. Asakura, M. Tsukada, *J. Raman Spectrosc.* **2001**, *32*, 103; b) H. G. M. Edwards, D. W. Farwell, *J. Raman Spectrosc.* **1995**, *26*, 901; c) P. Monti, G. Freddi, A. Bertoluzza, N. Kasai, M. Tsukada, *J. Raman Spectrosc.* **1998**, *29*, 297; d) Z. Shao, R. J. Young, F. Vollrath, *Int. J. Biol. Macromol.* **1999**, *24*, 295; e) J. Sirichaisit, V. L. Brookes, R. J. Young, F. Vollrath, *Biomacromolecules* **2003**, *4*, 387; f) T. Lefevre, M. Rousseau, M. Pezolet, *Biophys. J.* **2007**, *92*, 2885; g) J. B. Addison, N. N. Ashton, W. S. Weber, R. J. Stewart, G. P. Holland, J. L. Yarger, *Biomacromolecules* **2013**, *14*, 1140; h) T. Asakura, Y. Suzuki, Y. Nakazawa, G. P. Holland, J. L. Yarger, *Soft Matter* **2013**, *9*, 11440; i) J. M. Kenney, D. P. Knight, C. Dicko, F. Vollrath, in *Proc. of the 19th European Colloquium of Arachnology* (Eds.: S. Toft, N. Scharff), Aarhus University Press, Aarhus, Denmark **2000**; j) C. Dicko, D. Knight, J. M. Kenney, F. Vollrath, *Biomacromolecules* **2004**, *5*, 758; k) A. Martel, M. Burghammer, R. J. Davies, E. D. Cola, C. Vendrely, C. Riekel, *J. Am. Chem. Soc.* **2008**, *130*, 17070; l) C. Riekel, F. Vollrath, *Int. J. Biol. Macromol.* **2001**, *29*, 203; m) D. Sapede, T. Seydel, V. T. Forsyth, M. M. Koza, R. Schweins, F. Vollrath, C. Riekel, *Macromolecules* **2005**, *38*, 8447; n) I. Greving, C. Dicko, A. Terry, P. Callow, F. Vollrath, *Soft Matter* **2010**, *6*, 4389; o) M. Boulet-Audet, F. Vollrath, C. Holland, *J. Exp. Biol.* **2015**, *218*, 3138; p) U. Slotta, M. Tammer, F. Kremer, P. Koelsch, T. Scheibel, *Supramol. Chem.* **2006**, *18*, 465; q) S. Ling, Z. Qi, D. P. Knight, Z. Shao, X. Chen, *Polym. Chem.* **2013**, *4*, 5401; r) G. Fang, S. Sapru, S. Behera, J. Yao, Z. Shao, S. C. Kundu, X. Chen, *J. Mater. Chem. B* **2016**, *4*, 4337; s) J. Guan, D. Porter, F. Vollrath, *Polymer* **2012**, *53*, 2717; t) J. Guan, D. Porter, F. Vollrath, *Biomacromolecule* **2013**, *14*, 930; u) B. Mortimer, J. Guan, C. Holland, D. Porter, F. Vollrath, *Acta Biomater.* **2015**, *11*, 247; v) J. Guan, Y. Wang, B. Mortimer, C. Holland, Z. Shao, D. Porter, F. Vollrath, *Soft Matter* **2016**, *12*, 5926.

[5] a) D. Porter, F. Vollrath, *Nanotoday* **2007**, *2*, 6; b) D. Porter, F. Vollrath, *Soft Matter* **2008**, *4*, 328; c) D. Porter, F. Vollrath, *Adv. Mater.* **2009**, *21*, 487; d) D. Porter, F. Vollrath, *Polymer* **2009**, *50*, 5623; e) D. Porter, F. Vollrath, *Biochim. Biophys. Acta, Proteins Proteomics* **2012**, *1824*, 785; f) F. Libonati, M. J. Buehler, *Adv. Eng. Mater.* **2017**, *19*, 1600787.

[6] A. Sponner, E. Unger, F. Grosse, K. Weisshart, *Nat. Mater.* **2005**, *4*, 772.

[7] a) S. R. Koebley, F. Vollrath, H. C. Schniepp, *Mater. Horiz.* **2017**, *4*, 377; b) C. P. Brown, J. Macloed, H. Amenitsch, F. Cacho-Nerin, H. S. Gill, A. J. Price, *Nanoscale* **2011**, *3*, 3805.

[8] a) T.-Y. Lin, H. Masunga, R. Sato, A. D. Malay, K. Toyooka, H. Takaaki, K. Numata, *Biomacromolecules* **2017**, *18*, 1350; b) L. D. Miller, S. Putthanarat, R. K. Eby, W. W. Adams, *Int. J. Biol. Macromol.* **1999**, *24*, 159; c) S. Putthanarat, N. Stribeck, S. A. Fossey, R. K. Eby, W. W. Adams, *Polymer* **2001**, *41*, 7735; d) F. Zhang, Q. Lu, J. Ming, H. Dou, Z. Liu, B. Zuo, M. Qin, F. Li, D. L. Kaplan, X. J. Zhang, *J. Mater. Chem. B.* **2014**, *2*, 3879; e) S. Ling, C. Li, K. Jin, D. L. Kaplan, M. J. Buehler, *Adv. Mater.* **2016**, *28*, 7783; f) S. Ling, K. Jin, D. L. Kaplan, M. J. Buehler, *Nano Lett.* **2016**, *16*, 3795.

[9] Y. G. Li, P. Zhang, Z. J. Ding, *Scanning* **2013**, *35*, 127.

[10] R. C. Master, A. J. Pearson, T. S. Glen, F. C. Sasam, L. Li, M. Dapor, A. M. Donald, D. G. Lidzey, C. Rodenburg, *Nat. Commun.* **2015**, *6*, 6928.

[11] a) N. Qin, S. Zhang, J. Jiang, S. G. Corder, Z. Qian, Z. Zhou, W. Lee, K. Liu, X. Wang, X. Li, Z. Shi, Y. Mao, H. A. Bechtel, M. C. Martin, X. Xia, B. Marelli, D. L. Kaplan, F. G. Omenetto, M. Liu, T. H. Tao, *Nat. Commun.* **2016**, *7*, 13079; b) M. Boulet-Audet, F. Vollrath, C. Holland, *J. Exp. Biol.* **2015**, *218*, 3138; c) P. Monti, P. Taddei, G. Freddi, T. Asakura, M. Tsukada, *J. Raman Spectrosc.* **2001**, *32*, 103; d) C. Riekel, F. Vollrath, *Int. J. Biol. Macromol.* **2001**, *29*, 203; e) D. Porter, F. Vollrath, *Adv. Mater.* **2009**, *21*, 487; f) G. Fang, S. Sapru, S. Behera, J. Yao, Z. Shao, S. Kundu, X. Chen, *J. Mater. Chem. B* **2016**, *4*, 4337.

[12] Q. Wan, R. C. Masters, D. Lidzey, K. J. Abrams, M. Dapor, R. A. Plenderleith, S. Rimmer, F. Claeyssens, C. Rodenburg, *Ultramicroscopy* **2016**, *171*, 126.

[13] a) Z. Shao, F. Vollrath, J. Sirichaisit, R. J. Young, *Polymer* **1999**, *40*, 2493; b) D. T. Grubb, G. D. Ji, *Int. J. Biol. Macromol.* **1999**, *24*, 203; c) T. Lefevre, M. E. Rousseau, M. Pezolet, *Biophys. J.* **2007**, *92*, 2885; d) Y. Kawahara, A. Nakayama, N. Matsumura, T. Yoshioka, M. J. Tsuji, *Appl. Polym. Sci.* **2008**, *107*, 3681.

[14] a) S.-J. He, R. Valluzzi, S. P. Gido, *Macromolecules* **1999**, *24*, 187; b) M. Boulet-Audet, F. Vollrath, C. Holland, *J. Exp. Biol.* **2015**, *218*, 3138; c) D. Sapede, T. Seydel, V. T. Forsyth, M. M. Koza, R. Schweins, F. Vollrath, C. Riekel, *Macromolecules* **2005**, *38*, 8447.

[15] Y. Shen, M. A. Johnson, D. C. Martin, *Macromolecules* **1998**, *31*, 8857.

[16] a) D. N. Breslauer, L. P. Lee, S. J. Muller, *Biomacromolecules* **2009**, *10*, 49; b) M. Boulet-Audet, F. Vollrath, C. Holland, *Phys. Chem. Chem. Phys.* **2011**, *13*, 3979; c) M. Boulet-Audet,

© 2017 The Authors. Published by WILEY-VCH Verlag GmbH & Co. KGaA, Weinheim

A. E. Terry, F. Vollrath, C. Holland, *Acta Biomater.* **2014**, *10*, 776; d) C. Riekel, M. Mueller, F. Vollrath, *Macromolecules* **1999**, *32*, 4464; e) C. Holland, J. Urbach, D. Blair, *Soft Matter* **2013**, *8*, 2590.

[17] a) T. Asakura, K. Umemura, Y. Nakazawa, H. Hirose, J. Higham, D. Knight, *Biomacromolecules* **2007**, *8*, 175; b) T. Asakura, J. Yao, M. Yang, Z. Zhu, *Polymer* **2007**, *48*, 2064; c) K. H. Lee, *Macromol. Rapid Comm.* **2004**, *25*, 1792; d) C. S. Ki, I. C. Um, Y. H. Park, *Polymer* **2009**, *50*, 4618; e) M. Moriya, K. Ohgo, Y. Masubuchi, T. Asakura, *Polymer* **2008**, *49*, 952; f) M. Moriya, F. Reschzttadtz, Y. Nakahara, H. Saito, Y. Masubuchi, T. Asakura, *Biomacromolecules* **2009**, *10*, 929; g) D. N. Breslauer, L. P. Lee, S. J. Muller, *Biomacromolecules* **2009**, *10*, 49; h) C. Holland, D. Porter, F. Vollrath, *Biopolymers* **2012**, *97*, 362; i) K. Tanaka, S. Mizuno, *Insect Biochem. Mol. Biol.* **2001**, *31*, 665; j) Y. Liu, Z. Shao, F. Vollrath, *Nat. Mater.* **2005**, *4*, 901.

[18] a) S. Keten, Z. Xu, B. Ihle, M. J. Buehler, *Nat. Mater.* **2010**, *9*, 359; b) A. Nova, S. Keten, N. M. Pugno, A. Redaelli, M. J. Buehler, *Nano Lett.* **2010**, *10*, 2626.

[19] a) G. H. Michler, H.-H. K.-B. Von Schmeling, *Polymer* **2013**, *54*, 3131; b) Z. Huang, Y. Zhang, A. Motak, S. Ramakrishna, *Compos. Sci. Technol.* **2003**, *63*, 2223; c) J. Sandler, P. Werner, M. S. Shaffer, V. Demchuk, V. Altstadt, A. H. Windle, *Composites, Part A* **2002**, *33*, 1033; d) K. Lozano, E. V. Barrera, *J. Appl. Polym. Sci.* **2001**, *79*, 125; e) S. W. Cranford, *J. R. Soc., Interface* **2013**, *10*, 20130148; f) S. Isabelle, J. B. Markus, *Nanotechnology* **2016**, *27*, 302001.

[20] R. M. Robson, *Int. J. Biol. Macromol.* **1999**, *24*, 145.

[21] M. Kitagawa, T. Kitayama, *J. Mater. Sci.* **1997**, *32*, 2005.

[22] D. C. Joy, M. S. Prasad, H. M. Meyer III, *J. Microsc.* **2004**, *215*, 77.

[23] C. Rodenburg, M. A. E. Jepson, E. G. T. Bosch, M. Dapor, *Ultramicroscopy* **2010**, *110*, 1185.

© 2017 The Authors. Published by WILEY-VCH Verlag GmbH & Co. KGaA, Weinheim